




Imaging technologies for cardiac fiber and heart failure: a review

Shana R. Watson¹ · James D. Dormer¹ · Baowei Fei^{1,2,3,4,5} 

Published online: 2 March 2018

© Springer Science+Business Media, LLC, part of Springer Nature 2018

Abstract

There has been an increasing interest in studying cardiac fibers in order to improve the current knowledge regarding the mechanical and physiological properties of the heart during heart failure (HF), particularly early HF. Having a thorough understanding of the changes in cardiac fiber orientation may provide new insight into the mechanisms behind the progression of left ventricular (LV) remodeling and HF. We conducted a systematic review on various technologies for imaging cardiac fibers and its link to HF. This review covers literature reports from 1900 to 2017. PubMed and Google Scholar databases were searched using the keywords “cardiac fiber” and “heart failure” or “myofiber” and “heart failure.” This review highlights imaging methodologies, including magnetic resonance diffusion tensor imaging (MR-DTI), ultrasound, and other imaging technologies as well as their potential applications in basic and translational research on the development and progression of HF. MR-DTI and ultrasound have been most useful and significant in evaluating cardiac fibers and HF. New imaging technologies that have the ability to measure cardiac fiber orientations and identify structural and functional information of the heart will advance basic research and clinical diagnoses of HF.

Keywords Heart failure · Cardiac fiber · Myofiber · Medical imaging · Magnetic resonance imaging (MRI) · MR diffusion tensor imaging · Ultrasound imaging

Abbreviations

ADC	Apparent diffusion coefficient
ARE	Average relative error
BTI	Backscatter tensor imaging
CRT	Cardiac resynchronization therapy
CT	Computerized tomography
DSC	Dice similarity coefficient
DSI	Diffusion spectrum imaging
DTI	Diffusion tensor imaging

ETI	Elastic tensor imaging
FA	Fractional anisotropy
HF	Heart failure
LDDMM	Large deformation diffeomorphic metric mapping
LV	Left ventricle; left ventricular
MRI	Magnetic resonance imaging
NMR	Nuclear magnetic resonance
PET	Positron emission tomography
PS	Polarized sensitive
OCT	Optical coherence tomography
RVFW	Right ventricular free wall
SHG	Second harmonic generation
SPECT	Single photon emission computed tomography
SWI	Susceptibility weight imaging
TPM	Two photon microscopy

✉ Baowei Fei
 bfei@emory.edu; <http://www.fei-lab.org>

¹ Department of Radiology and Imaging Sciences, Emory University School of Medicine, Atlanta, GA, USA

² Winship Cancer Institute of Emory University, Atlanta, GA, USA

³ Department of Mathematics and Computer Science, Emory University, Atlanta, GA, USA

⁴ Department of Biomedical Engineering, Emory University and Georgia Institute of Technology, Atlanta, GA, USA

⁵ Quantitative Bioimaging Laboratory, Department of Radiology and Imaging Sciences, School of Medicine, Emory University, Atlanta, United States

Introduction

Cardiovascular imaging has been widely used in basic sciences and clinical applications due to its ability to provide a detailed description of the heart structure and function [1]. A hallmark of several cardiac pathologies is remodeling of the left ventricle (LV) geometry and changes

in cardiac fiber orientation [2, 3], each of which can be visualized using various imaging modalities [4–13]. Descriptive datasets generated using imaging techniques are often analyzed and quantified to provide a diagnosis or are utilized for comparison of healthy versus diseased tissue states.

Cardiac fibers are long, cylindrical muscle cells with one or two nuclei. The cardiac fibers or cardiac myofibers form a complex, three-dimensional network that is packed with contractile elements. Orientation of cardiac fibers has an important role in determining the LV pump function [14, 15] and cardiac electrophysiological and mechanical properties [16–19], both of which make it critical in the study of heart failure (HF). Advances in high-resolution imaging and improvements in image registration make it easier to identify changes in cardiac microstructures. In this study, we intend to provide an overview of imaging methodologies and their capability to visualize cardiac fibers for the study of HF.

This review covers literature reports from 1900 to 2017. PubMed and Google Scholar databases were searched using the keywords “cardiac fiber” and “heart failure” or “myofiber” and “heart failure.” Searches were not confined to a date range. We provide a thorough examination of the imaging methodologies that have been set forth to study cardiac fibers. The application section is dedicated to describing the usefulness of imaging to determine cardiac fiber orientation. We conclude with the direction of future research and the challenges of using imaging to assess HF severity.

Pathology of heart failure

HF is described as a complex syndrome characterized by inability of the heart to supply sufficient cardiac output to meet the metabolic needs of the body [20]. HF begins with myocardial injury that results in a loss of a critical quantity of myocardial cells [21]. Common etiologies are ischemic heart disease, CAD, diabetes, and hypertension [21]. Less common causes are cardiomyopathies [22], infections, toxins, valvular diseases, and prolonged arrhythmias [21].

There are four different stages of HF as described by the American Heart Association which include:

- Stage A: no structural changes of the heart or presence of HF symptoms.
- Stage B: structural changes present but no HF symptoms.
- Stage C: both structural changes and HF symptoms are present.
- Stage D: symptoms are refractory and specialized treatment is required.

Features of heart failure

LV dilation

The LV is the main pumping chamber of the heart and when damaged/enlarged has an inability to supply an adequate amount of blood to tissues and organs of the body. LV dilatation is a well-recognized precursor of LV dysfunction; however, its effect on the risk of HF in individuals initially free of myocardial infarction is unknown [23]. Most studies showing LV dilation are historically conceptualized as dilated cardiomyopathy.

LV hypertrophy/remodeling

While the underlying causes of HF are multifactorial, myocyte hypertrophy and fibrosis are major contributors [24, 25]. LV remodeling characterized by hypertrophy and extracellular matrix (ECM) accumulation causes increased myocardial stiffness and impaired diastolic performance [26–29]. LV hypertrophy, which leads to LV dysfunction contributes to disease progression, pressure overload, or volume overload. LV diastolic dysfunction and LV hypertrophy have been observed in systolic HF. Other attributes of systolic HF include dilated cardiomyopathies [30] and reduction in muscle mass [31].

Preserved ejection fraction

LV remodeling characterized by LV hypertrophy and ECM accumulation (myocardial fibrosis) causes increased myocardial stiffness and impaired diastolic dysfunction despite having a relatively normal ejection fraction. This is called HF with preserved ejection fraction (HFpEF) and can compromise 50% or more of HF presentations/admissions. Through functional imaging, it has been established that a structural adversity in the progression of HFpEF is ECM remodeling [32–37].

Diastolic dysfunction

Diastolic dysfunction refers to an abnormal LV relaxation during echocardiographic measurements [38]. It is characterized by impairment in diastolic filling, prolongation of isovolumetric relaxation, and increased atrial filling [39]. In animal models, diastolic dysfunction is shown to be the first sign of contractile failure [39]. Hemodynamic studies performed showed a normal ejection fraction, suggesting a preservation of systolic function but a decrease in end-diastolic volume, signifying abnormal diastolic function. Types of diastolic dysfunction HF are increased LV stiffness, infiltrative myocardial diseases, mitral or tricuspid valve stenosis, and pericardial disease.

Cardiac fiber and heart failure

Cardiac fibers in the heart

There has been a detailed investigation of the fiber structure of the LV wall, and the smooth transition of fiber angles from endocardium to epicardium has also been emphasized [40]. Cardiac fibers are arranged in layers of counter-wound helices around the ventricles [40–45], as shown in Fig. 1. The complex structural organization of cardiac fibers and the spatial arrangement of cardiomyocytes in laminar sheetlets significantly contribute to cardiac function and contractile ejection patterns [14]. Indirect estimation of local cardiac fiber orientation using the procedure of mapping the cardiac fiber from DTI data has been done by MRI and ultrasound [16, 46, 47].

For describing the global arrangement, most studies and computational models have depicted the LV myocardial architecture as a transmural continuum between two, helical fiber geometries, where right-handed helical geometry in the subendothelial region gradually changes into left-handed geometry in the subepicardial region, as shown in Fig. 2 [48].

Normal human LV architecture comprises a highly aligned array of cardiac fibers whose orientation depends on the transmural location [49]. The spatial relations of the fibers in serial microscopic sections suggest that the LV, for purposes of stress analysis, can be characterized as a cross-linked, fiber-wound, ellipsoidal, or paraboloidal pressure vessel with the fiber angle changing smoothly from approximately 60° at the endocardium to approximately -60° at the epicardium [40]. The LV geometry and fiber structure are known to be remodeled in many disease processes [50].

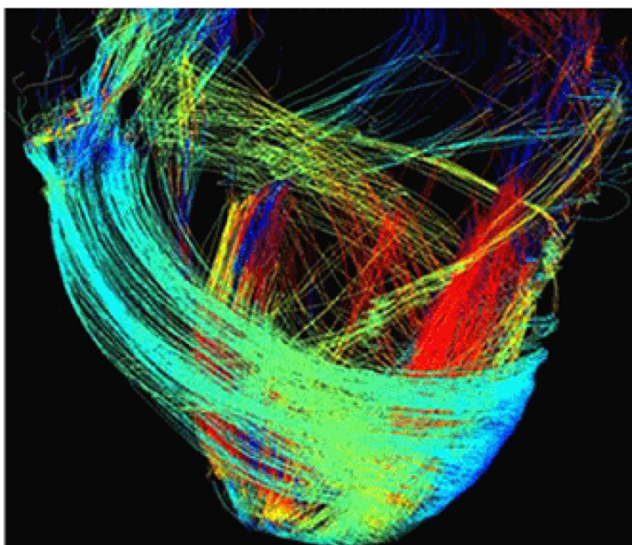


Fig. 1 Representative image of cardiac fiber tracing in a canine heart using MR-DTI. Image adapted from [3]

Cardiac fiber organization in the diseased heart

Fuster et al. quantified LV myocardial fiber hypertrophy and interstitial tissue into four groups of patients who were free of coronary disease: (1) 22 normal hearts, (2) 20 hearts from patients with mitral incompetence (postpartum due to causes other than HF), (3) 22 hearts from patients with mitral incompetence (postpartum due to HF from low cardiac output syndrome, and (4) 22 hearts from patients with hypertensive heart disease [51]. These researchers showed that the average myocardial fiber diameters in groups 2, 3, and 4 were higher than that of normal hearts (group 1) [51]. This study suggested that there is a difference in the myocardial fiber structure between healthy and diseased hearts.

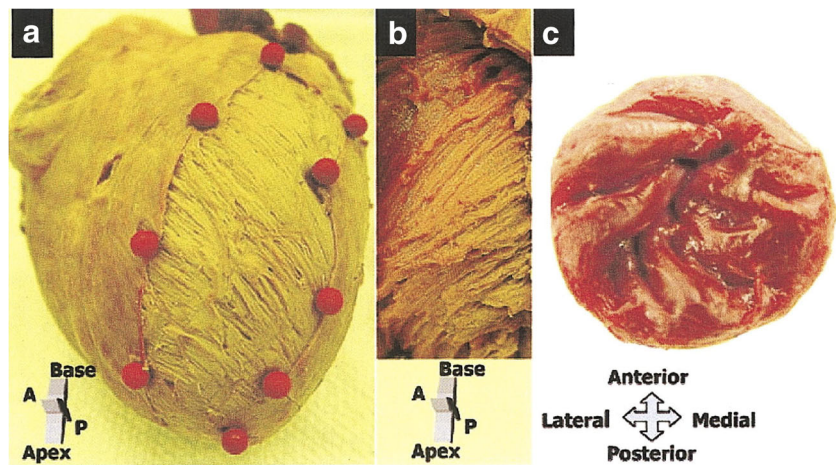
Geerts-Ossevoort et al. used MR-DTI to determine cardiac fiber orientations in normal and infarcted goat hearts [52]. Their results contradicted previous and subsequent studies which stated that fiber structure correlated with infarct size and left LV function [53] or is remodeled in disease processes [50, 51]. Geerts-Ossevoort et al. suggest that the fiber structure remains preserved in the presence of a transmural myocardial infarction based on the analysis of three goat hearts [52].

Cardiac fibers and stress analyses

Streeter proposed a model for stress analysis of the LV wall based on the realistic assumption that the myocardium is essentially composed of fiber elements that have only axial tension and vary in orientation throughout the wall [54]. This model required an extensive study of muscle fiber orientation and curvature through the myocardium. The wall was regarded as a tethered set of nested shells with a unique fiber orientation. Results from this pioneering model indicate that (a) fiber curvature is maximum at midwall at the end systole; (b) the pressure through the wall decreases more rapidly near the endocardium than near the epicardium at the end diastole, even when a constant tension is assumed for each fiber through the wall; (c) at the end diastole, the curve for the circumferential stress versus wall thickness is convex with maximum thickness at the midwall; and (d) the curvature and stress distributions obtained by direct measurements at a selected local site agree with the computed “ellipsoid” data [54].

In a study of 66 patients in sinus rhythm, equatorial and longitudinal LV wall stress was calculated at the end diastole [55]. Of these patients, 31 had volume overload, six had acute and 21 had chronic aortic incompetence, and four had chronic mitral incompetence. Another four patients served as the control, six patients had aortic stenosis, and 25 had congestive cardiomyopathy. In the patients with volume overload and congestive cardiomyopathy, LV dilation was accompanied by an increase in wall thickness so that the stress conversion factor, i.e., the factor relating pressure to stress, was normal and the absolute stress depended on the end-diastole pressure

Fig. 2 Depiction of the helical arrangement of muscle fibers in the LV of an explanted adult porcine heart. The arrangement of cardiac fibers is shown in a circumferential-longitudinal plane which changes from a left-handed helix in the subepicardium (a) to a right-handed helix in the subendocardium (b). The helical arrangement of the endocardial region is also reflected in the arrangement of trabeculae near the apex (c). A: anterior; P: posterior. Reprinted from Reference [48]



[55]. In pressure overload of the LV (aortic stenosis), the increase in wall mass reduced the stress conversion factor so that absolute fiber stress was normal. These data support the hypothesis that cardiac fiber stress may be an important determinant of LV hypertrophy [55].

Overview of imaging technologies for detecting heart failure and cardiac fibers

Overview of imaging for heart failure

Various imaging technologies were developed to characterize the conditions of heart diseases including HF. Cardiac imaging has been used in the study of a variety of medical conditions and has become a necessary tool for patient diagnosis and follow-up [1]. Three-dimensional imaging techniques have the capability to improve heart disease diagnosis and outcomes. Among the cardiac imaging systems are also ultrasound [56–58], chest X-ray [59, 60], cardiac catheterization [61, 62], magnetic resonance imaging (MRI) [52, 63, 64], computerized tomography (CT) [65, 66], cardiac positron emission tomography (PET) [67–69], cardiac single-photon emission computed tomography (SPECT) [70], and intravascular ultrasound [71, 72]. Ultrasound allows for non-invasive visualization of blood flow through the heart using Doppler [73]. MRI differentiates soft tissues better than CT and can obtain information regarding the size, morphology, and characteristics of tissue in a single session [74, 75].

Ultrasound and MR-DTI are the most popular imaging tools for evaluating HF. Some animal models that have been used with these imaging protocols for HF studies are rat [76, 77], canine [2, 10, 50, 78, 79], rabbit [12, 80], pig [81], sheep [56, 80, 82], and mice [14, 83]. Figure 3 shows representative DT-MRI images of hearts from a mouse, a rabbit, and a sheep. Each specimen

shows cardiac fiber orientations (A, B, C) which would be useful for clinical study. There is a promising future for cardiac fiber imaging with MRI as more efficient scans become available [84, 85].

Overview of imaging for cardiac fibers

Techniques that have been explored to view cardiac fibers include microscopy and macroscopy techniques (Fig. 4) which are also capable of visualizing LV septum. Other important imaging tools are histology [12, 78, 86], optical coherence tomography (OCT) [11, 17, 87, 88], multimodality imaging [16, 89, 90], second-harmonic generation (SHG) microscopy [10, 91], and susceptibility weight imaging (SWI) [92]. Table 1 provides a summary of the imaging methodologies that have been used to evaluate cardiac fiber arrangement in different species.

There are clinical needs to develop adequate models of LV architecture for various cardiac applications [42]. Research efforts and recent advances in imaging techniques have been dedicated to study the architecture of the heart [98].

An imaging tool with the capability to distinguish microstructural details of cardiac fiber organization is valuable for basic science and clinical applications [63, 99]. Imaging and quantifying fiber orientations in the heart is challenging [100]. At the light-microscopic level, the heart was described as a “sandwich” for which cardiac fibers in the middle layer run mainly circumferentially [8]. McLean et al. observed a “sleeve” in the interventricular septum formed by longitudinal and oblique cardiac fibers [8]. Although not a commonly used system in this field of study, the data from the light-microscope provided a quantitative description at the cellular level of cardiac fiber orientation throughout the LVs of the mouse heart.

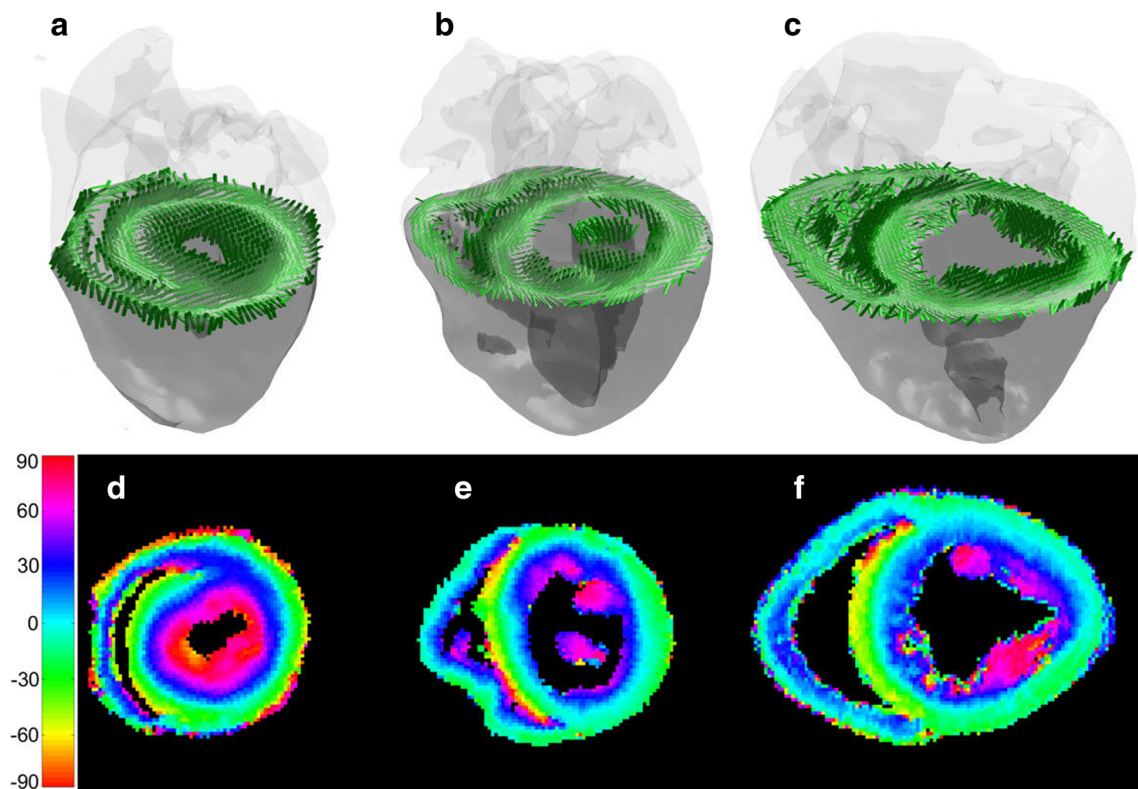


Fig. 3 Visualization of cardiac fiber orientation for representative mouse (a, d), rabbit (b, e), and sheep (c, f) heart specimens. The cardiac fibers from the same short axis are shown as rendered cylindrical rods (a–c)

inside semi-opaque volumes of the hearts viewed obliquely from an elevated perspective, or as false color-coded, helix angle maps. Adapted from Reference [80]

In vitro cardiac fiber imaging using MR-DTI

Normal heart

MRI has been implemented in order to acquire images of the myocardial fiber orientation field in the beating heart. MR-DTI emerged as a promising imaging tool for revealing myocardial orientation in 3D, although its long data acquisition duration limits its application to in vivo studies [92]. Its advantages are that it can measure fiber organization in isolated, perfused, arrested hearts, while avoiding fixation, staining,

and sectioning artifacts [12]. Histology requires all of the aforementioned, but remains the oldest and the gold standard for fiber orientation studies.

Mouse animal model

In order to investigate the validity and practicality of pattern-based analysis, Merchant et al. used 3D MR-DTI on 13 fixed mouse hearts [83]. Fiber angles in the LV were set to parametric expressions constructed from elementary functions of the prolate spheroidal spatial variables. It was determined that on

Fig. 4 Image depicts bilayered disposition of the cardiac fibers in the LV septum observed by optical microscopy and macroscopy. Image adapted from [6]

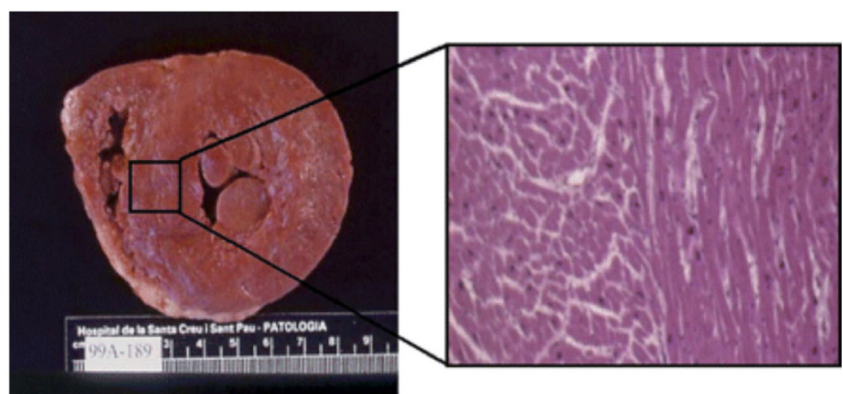


Table 1 Summary of imaging methodologies and the application of each to investigating cardiac fiber orientation

Reference	Imaging method	Application	Study size	Study summary
Hsu et al. [78]	MR-DTI	Canine myocardium	–	High-resolution MR fiber orientation mapping can be directly and quantitatively compared with results obtained from histology.
Scollan et al. [12]	MR-DTI	Rabbit hearts	7	Found that there is a level of organization beyond the fibers termed the laminar organization of the LV myocardium.
Beg et al. [93]	MR-DTI	Canine hearts	4	Provided mathematical and computational techniques for transforming cardiac ventricular anatomies to a coordinate system for quantitative analyses of geometry and fiber structure at corresponding locations.
Helm et al. [3]	MR-DTI	Normal (11) and failing (7) canine hearts	18	Directly compared the testing of a model and experimental results which can provide quantitative measurements, modeling, and investigation of ways that remodeling of LV micro-anatomy influences electrical conduction in the heart.
Chen et al. [76]	MR-DTI	Rat hearts	21	Found that geometric changes in both sheet and cardiac fiber orientations provide a substantial mechanism for radial wall thickening independent of components related to fiber shortening. Sheet reorientations are a primary determinant of myocardial wall thickening.
Helm et al. [2]	MR-DTI	Normal (8) and failing (5) canine hearts	13	Combined MR-DTI to computational anatomy imaging to demonstrate quantitatively global and local remodeling in normal and failing hearts with a left bundle branch block.
Carreras et al. [6]	MR-DTI ultrasound	Various cardiac images	–	Concluded that myocardial helical fiber orientation influences mechanical behavior and there is evidence of the double-loop, single muscular band model described by Torrent-Guasp.
Wu et al. [53]	MR-DTI	Mid-ventricular level of human hearts	37	Concluded that there is redistribution of fiber architecture after MI correlated with infarct size and LV function.
Rohmer et al. [44]	MR-DTI	Human hearts	–	Developed a visualization algorithm to demonstrate the 3D orientation of fibers and sheets in the human myocardium.
Crosby et al. [81]	Ultrasound	Porcine heart images	–	Examined the effect of including tissue anisotropy in simulated ultrasound images of the heart.
Kung, et al. [82]	MR-DTI	Sheep LV	6	Detected two local sheet populations throughout LV myocardium using MR-DTI and histology methods.
Lekadir et al. [94]	MR-DTI	Canine myocardial images	–	Improved cardiac fiber orientation modeling and prediction.
Vadakkumpadan et al. [79]	MR-DTI	Normal (6) and failing (3) canine hearts	9	Determined that there are no significant differences between estimated and acquired fiber orientations at a clinically observable level.
Milne et al. [56]	MR-DTI, ultrasound	Sheep hearts	7	Demonstrated that measurements of fiber orientation for individual hearts can be derived from ultrasound images.
Qin et al. [90]	High-frequency ultrasound	Phantoms and porcine hearts	–	Proposed a method to extract cardiac fiber orientations from high-frequency ultrasound.
Qin et al. [46]	MR-DTI, ultrasound	Rat (2) and canine (3) hearts	5	Provided cardiac fiber orientations to ultrasound images and demonstrated the ability to simulate electricity activations during the CRT process.
Angeli et al. [14]	MR-DTI	Mouse hearts	5	Constructed a tensor map to provide a description of the average fiber architecture.
Genet et al. [95]	MR-DTI	LV of human hearts	5	Obtained stress measurements which can serve as targets for in silicon design of heart failure treatments.
Qin et al. [96]	High-frequency ultrasound	Porcine hearts	–	Demonstrated the feasibility of extracting cardiac fiber orientations from high-frequency ultrasound images ex vivo and demonstrated the ability to measure cardiac fibers in vivo.
Qin et al. [97]	MR-DTI, ultrasound	Cardiac ultrasound images of rat hearts	50	Developed a simulation method to simulate cardiac ultrasound images of the heart using high-resolution MR-DTI data.
Qin et al. [77]	MR-DTI, ultrasound	Rat heart images	6	Investigated the registration between cardiac fiber orientations from a 3D MR-DTI (ex vivo) volume and 2D ultrasound images (in vivo).
Qin et al. [16]	MR-DTI, ultrasound	Rat hearts	3	Demonstrated the feasibility of using ultrasound to estimate the orientation of in vivo beating hearts.
Qin et al. [16]	Ultrasound	Rat heart	1	Provided a cardiac ultrasound imaging and fiber orientation estimation technique.
Dormer et al. [89]	Ultrasound and MR-DTI	Rat hearts	5	Proposed a new approach to generate cardiac fiber orientation that may be used for multiple cardiac applications.
Merchant et al. [83]	MR-DTI	Mouse hearts	13	Demonstrated that parametric models can predict the 3D cardiac fiber structure from a finite number of 2D slices.

Note: MR-DTI indicates magnetic resonance diffusion tensor imaging; MI indicates myocardial infarction; LV indicates left ventricle or left ventricular; CRT indicates cardiac resynchronization therapy

average, the myocardial fiber helix angle can be represented to 6.5° accuracy by the equivalence of a product of 10th-order polynomials of the radial and longitudinal variables and 17th-order Fourier series of the circumferential variable [83]. Similarly, the fiber imbrication angle was described by 10th-order polynomials and 24th-order Fourier series to 5.6° accuracy. However, the representations did not adversely affect the information commonly derived from DTI datasets. It was also demonstrated that parametric models can predict the 3D myocardial fiber structure from a finite number of 2D slices. These findings strongly support the principle of parametric modeling for characterizing myocardial structures [83].

Rat animal model

Chen et al. [76] used MR-DTI on 21 isolated, perfused Sprague-Dawley rat hearts arrested or fixed in three different conditions, i.e., (1) end diastole, (2) early systole, or (3) end systole. The primary eigenvectors of diffusion tensors can be used to determine the orientations at the base, mid-LV, and apex of the heart, whereas the sheet structure can be determined from the secondary and tertiary eigenvectors at the same location. It was observed that the cardiac fiber helix angle changed as contraction proceeded from the end diastole to the early systole. Endocardial and epicardial fibers became more longitudinally oriented in the end systole group. Although significant regional variations were exhibited by the sheet structure, changes in the sheet structure during contraction are fairly uniform across regions. There was evidence of a more radial orientation of the sheets during the early and end systoles. Chen et al. were the first to show that geometric changes in both sheet and fiber orientation provide a substantial mechanism for radial wall thickening which is independent of the active components due to fiber shortening [76]. These results show that sheet reorientation is a primary determinant of myocardial wall thickening.

Rabbit animal model

Scollan et al. [12] proposed a quantitative validation of the MR-DTI method for measuring cardiac fiber orientation. Fiber orientations were statistically compared in the same locations within the same hearts using MR-DTI and histology to compare in a total of two, perfused rabbit hearts. Fiber orientations were statistically similar for both methods and differed on an average by 12° at a single location (Fig. 5). This is similar to the 10° of uncertainty that is achieved with histological techniques. Studies prior to Scollan and colleagues most often observed a qualitative agreement of diffusion anisotropy with fiber orientation in the heart [101].

Canine animal model

Prior to the model described above was a similar LDDMM method based on Grenander's deformable template model [93]. This model was developed by Beg and colleagues [93] and was intended to transform heart geometry into coordinates for quantification of shape. This would be used to provide a mathematical and computation method for quantifying changes in the LV geometry and fiber orientation after it has undergone global or local remodeling. This group used two automated landmark placement methods for modeling tissue deformations expected in different cardiac pathologies. MR-DTI images of four male mongrel dogs were used. Fiber angles for the target hearts were computed using the template mesh with the inclusion of the large deformation diffeomorphic metric mapping (LDDMM)-generated transformation to identify the target voxels origination in the template finite element boundaries [93]. Registering the heart anatomies allowed for the properties of the heart to be quantified.

Helm et al. presented the LDDMM algorithm which suggested that this algorithm can be used to reconstruct hearts into correspondence so that the variability of the LV geometry, fiber, and sheet orientation can be quantified [3]. It was revealed that epicardial electrical mapping and MR-DTI imaging can be done in the same hearts. These results facilitated direct comparison and testing of model versus experimental results and allowed for quantitative measurement, modeling, and analysis of remodeling occurrence in the LV that influences electrical conduction in the heart [3]. A 3D diffusion-weighted imaging (DWI) method can be used to measure cardiac fibers at high spatial resolution, as shown by Helm et al. [50] This method was applied to the ex vivo reconstruction of seven canine hearts. The results of this study confirmed previous histological data which stated that the tertiary eigenvector of DT defines the sheet normal [50].

Lekadir et al. presented a statistical approach for the prediction of fiber orientation based on the myocardial morphology of the Knutsson mapping [94]. In this space, the orientation of each fiber was represented in a continuous and distance-preserving manner which allowed consistent statistical analysis of the data [94]. Furthermore, the directions in the shape space correlated mostly with the myocardial fiber orientations which were extracted and used for subsequent prediction [94]. All shape information in this model was taken into account in the analysis, and the obtained latent variables were statistically optimal for predicting fiber orientation in new datasets. The proposed technique is validated based on a sample of canine MR-DTI datasets, and the results demonstrated marked improvement in cardiac fiber orientation modeling and prediction [94].

Continuous improvement of MR-DTI methods will provide datasets with both geometry and fiber structure. In the

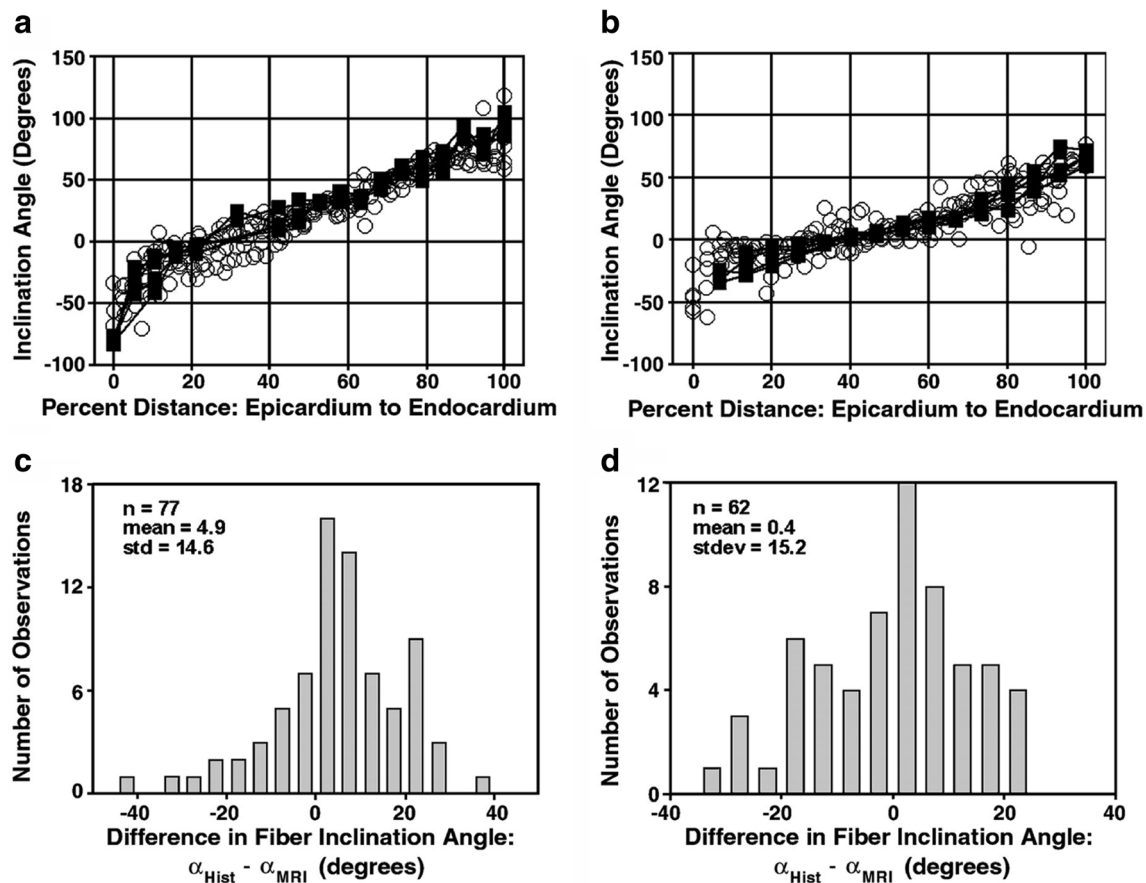


Fig. 5 **a** Fiber inclination angle measurements and primary eigenvector inclination angle estimates obtained from a spin-echo pulse sequence for a total of five, transmural locations in one heart. **b** Fiber inclination angle and primary eigenvector inclination angle estimates obtained in another

heart using the fast spin-echo pulse sequence. **c** Distribution of the differences in the fiber inclination angle at each voxel obtained using histology and spin-echo MR-DTI. **d** Constructed similar to C but for fast spin-echo heart. Reprinted from Reference 12

clinical setting, MRI is capable of acquiring patient-specific data regarding cardiac geometry [93].

Sheep animal model

MR-DTI was also performed on six sheep LVs and with corresponding, direct, histological, transmural measurements made within the anterobasal and lateral-equatorial LV [82]. Secondary and tertiary eigenvectors of the diffusion tensor were compared with each of the two, sheet orientations observed on histology [82]. The results showed a mean difference ± 1 SD between MR-DTI and histology of the measured sheet angles was $8^\circ \pm 27^\circ$ [82]. It was concluded that two, local, myocardial sheet populations existed throughout the LV myocardium, as confirmed by MR-DTI [82].

In vivo human studies

A study directly evaluating cardiac fibers in the presence of HF was produced by Genet et al. [95]. Reference maps were constructed of normal LV wall stress in humans that could be used as a target for in silico optimization studies of current and

future treatments for HF [95]. This group constructed and designed computational methods of the LVs of five, normal human patients using MR images and the finite element (FE) method. In each patient, LV data was extracted from MRI and validated through comparison with strain measurements from tagged MRI in order to calibrate these models. To avoid errors in measuring the volume due to LV motion, segmentation was performed in both the short and long axes [95]. The segmented contours were used to reconstruct the endocardial and epicardial surfaces, after which a hexahedral FE mesh of the LV wall was constructed (Fig. 6). The values obtained for the passive material parameter, end-diastolic, and end-systolic cardiac fiber stress fields could potentially serve as the reference for future construction of normal human LV computational models [95].

Ex vivo human studies

Experiments performed by Rohmer et al. reconstructed and visualized fiber and laminar structures in 3D [44]. Anisotropic, least square filtering followed by fiber and sheet tracking techniques was applied to MR-DTI data of the

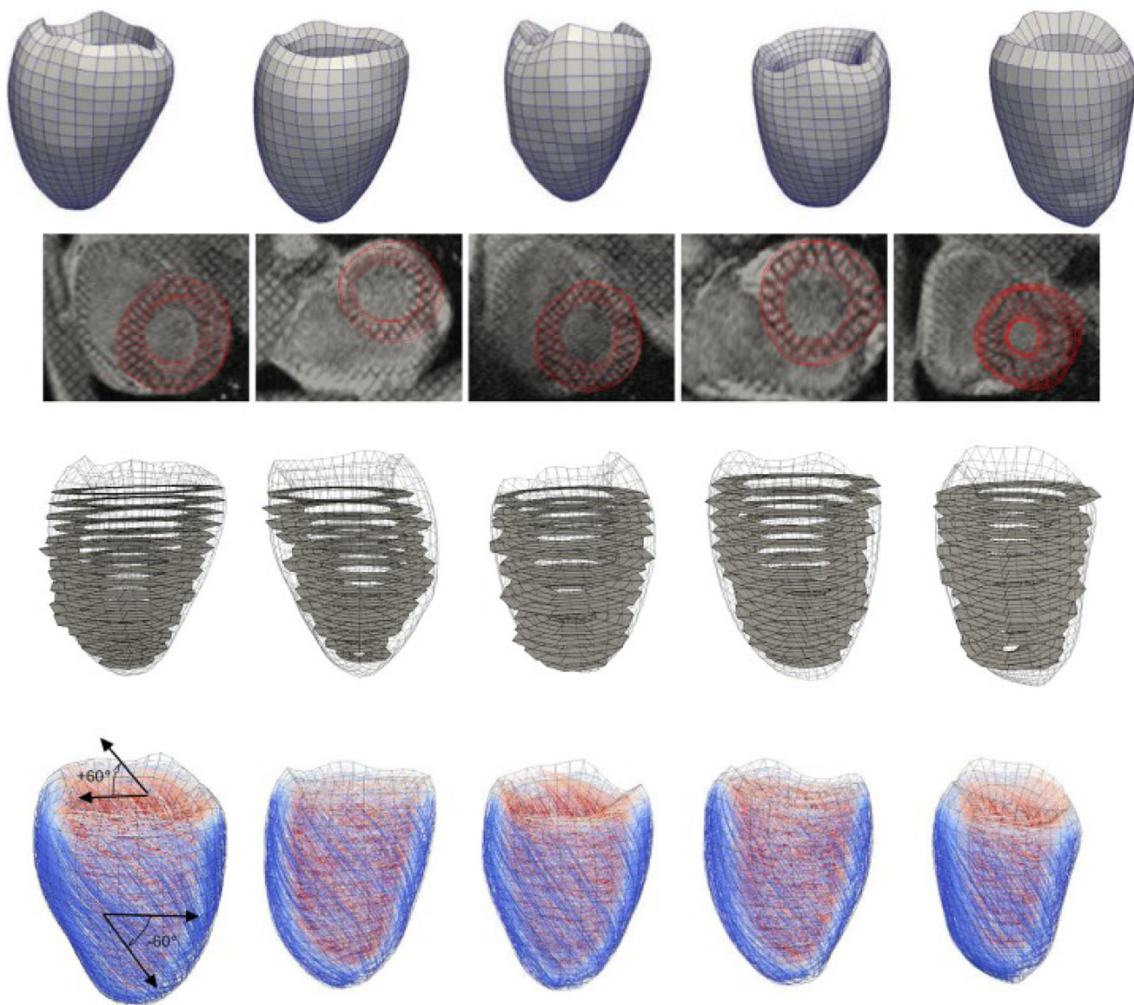


Fig. 6 First row: Subject-specific LV geometries (at the beginning of diastole) extracted from MR images. Second-row: match between FE meshes and the MR images. Third row: two-dimensional sectors used to compute strain from the tagged MR images, superimposed onto three-dimensional finite element images (shown as wire frames). Fourth

row: rule-based fiber orientation map. Color denotes helix angle with respect to the circumferential direction when viewed from epicardium (-60° , blue to $+60^\circ$, red), superimposed onto the FE meshes. The image was adapted from Reference [95].

excised normal human heart. Fibers and sheets were defined similar to those in Reference [60] [76]. Findings indicated that the fibers lie in sheets that have a transmural structure which corresponds to histologic studies published in the scientific literature. Quantitative measurements show that the sheets, as opposed to the fibers, are organized into laminar orientations without dominant populations. An algorithm was developed to demonstrate the complex 3D orientation of the fibers and sheets in human myocardium [44].

Ultrasound imaging

Ultrasound

Ultrasound techniques, such as tissue Doppler imaging, have an excellent temporal resolution (< 4 ms) and provide the

instantaneous velocity of myocardial motion [102]. The velocity data can be used for calculating parameters, such as the displacement, strain rate, and strain [102]. Therefore, cardiac ultrasound has an important role in the imaging of hearts in basic and clinical cardiovascular research [90] and remains the gold standard for cardiac function assessment. Ultrasound is often used in clinical cardiac examinations because it can provide real-time functional information regarding heart values and, similar to most three-dimensional imaging techniques, it has the capability to provide the geometry and motion information of the heart [103]. However, ultrasound cannot do so while supplying information regarding the cardiac fiber orientation [46]. Information regarding cardiac fibers must be wrapped to the ultrasound volume in order to supply useful information regarding the stress distributions and electric action spreading.

Information from two-dimensional (2D) ultrasound or angiography alone may not provide a complete picture of the heart, as reported earlier [100] and may lead to some misconceptions. 2D ultrasound only provides “flat” views of the heart and is fixed in terms of the piezoelectric element vertical dimension. Whereas 3D ultrasound involves real-time volumetric imaging that allows for acquisition of pyramidal datasets.

Acquiring 3D volumes of the heart of small animals *in vivo* for cardiac fiber wrapping is challenging, although a method was proposed to acquire 3D ultrasound volume for rat hearts *in vivo* after an open-chest surgical method (described in detail by Qin et al.) [77]. This method is promising for quantifying LV geometry and severe heart remodeling. Qin et al. used two steps to wrap cardiac fiber orientations from DTI to the target ultrasound geometries. Step 1 was to generate the deformation field between the ultrasound geometry of the heart and the MRI geometry of the template heart. Step 2 involved the application of a diffeomorphic Demons registration method to perform a deformable registration. During quantitative evaluation, the processed image is compared with the reference image using the Dice similarity coefficient (DSC) as the performance assessment score. The feasibility of imaging beating hearts *in vivo* was also tested and which may provide an alternative method to assess the 3D geometry of the hearts in small animals *in vivo* (Fig. 7).

Ultrasound was used along with mean arterial pressures to determine the strain index and wall stress in normal hearts of both patients and swine, i.e., swine with pacing-induced CHF and patients with dilated cardiomyopathies [104]. Paired values of the stress and strain index display little change over a large range of normal cardiac mass, although they deviate from this range during HF [104].

Combination of ultrasound and MR-DTI

MR-DTI techniques have been combined with other types of imaging, such as ultrasound [16, 77] or CT [79]. Based on MR-DTI heart data, Qin et al. [97] proposed a cardiac ultrasound image simulation method which utilized both the cardiac geometry and the fiber orientation information to simulate the anisotropic intensities in ultrasound images from rat hearts. Prior to the simulation procedure, geometry orientations were obtained from high-resolution, structural MRI data while fiber orientations of the heart were obtained from MR-DTI data. The simulation included two steps: (1) backscatter coefficients of the point scatters inside the myocardium were processed according to the fiber orientations using an anisotropic model and (2) the cardiac ultrasound images were simulated with anisotropic myocardial intensities [97]. This method was compared to two, non-anisotropic intensity methods using 50 B-mode ultrasound image volumes of five, different rat hearts. Lastly, the simulated images were compared with the ultrasound images of a diseased rat heart *in vivo*. A new segmental evaluation method was presented to validate the simulation results. The findings suggest that the average relative errors (AREs) of the five parameters, i.e., mean intensity, Rayleigh distribution parameter, and first, second, and third quartiles, were utilized as the evaluation metrics. The simulated images were quantitatively compared with real ultrasound images in both *ex vivo* and *in vivo* experiments, and this method can be used as a clinical application to generate cardiac ultrasound images with anisotropic intensities inside the myocardium [97].

Geometries of the heart extracted from MRI are translated to ultrasound by rigid and deformable registration [46]. Deformation fields take into account both geometries from MRI and ultrasound after registration. The cardiac fiber orientations imaged from DTI are mapped to ultrasound volumes in

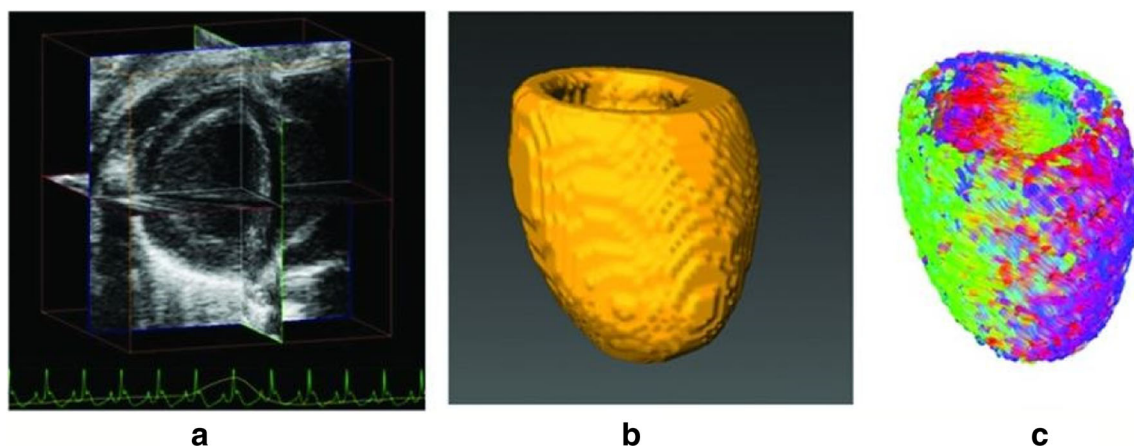


Fig. 7 Cardiac fiber orientation estimation of an *in vivo* beating heart. **a** 3D ultrasound volume *in vivo*. **b** Reconstructed cardiac geometry. **c** Estimated cardiac fiber orientations from the geometry. Image adapted from [47]

order to simulate electrical activations during the cardiac resynchronization therapy (CRT) process. This method was validated in two rat hearts and in three canine hearts. After MRI/ultrasound image registration, the DSC scores were greater than 90% and the corresponding target errors were less than 0.25 mm [46].

An MR-DTI, template-based framework developed by Qin et al. [16] was developed in order to estimate the cardiac fiber orientations from 3D ultrasound images using three, male, Sprague-Dawley rats. The cardiac fiber orientations of the target heart were estimated by deforming the fiber orientations of the template, based on the deformation field of the registration between the ultrasound geometry of the target heart and the MRI geometry of the template heart [16]. Four methods, i.e., DSC, target errors, acute angle error, and inclination angle error, were used to evaluate the method. The accuracy of cardiac fiber estimates was evaluated by a public database and then by their own database. The average values were $95.4\% \pm 2.0\%$ for the DSC of geometric registrations, $21.0^\circ \pm 0.76^\circ$ for the acute angle error, and $19.4^\circ \pm 1.2^\circ$ for the inclination angle error. Furthermore, this method showed a potential for understanding the dynamic mechanisms of the beating hearts due to its feasibility of performance on 3D ultrasound images of the beating heart [16].

Other imaging modalities

Specialized imaging approaches (Table 2) that have been used to visualize cardiac fibers include SHG imaging [91], optical polarization tomography (OPT) [99], and OCT [17],

polarized-sensitive (PS) OCT system [11]. In addition, for cardiac fiber detection, there are different modes that can be employed with MR-DTI. These include nuclear magnetic resonance (NMR) [101], diffusion spectrum imaging (DSI) [64], and DWI [50]. Sosnovik et al. reviewed the application of DSI in ischemic heart disease and provided in their conclusions that hardware limitations on most clinical scanners hinder the clinical translation of diffusion tractography in the heart [64]. However, in animal studies, the technique is capable of imaging the microstructure of the myocardium and which makes it very competitive to other imaging techniques. Figure 8 shows the DSI tractography of a normal rat heart showing the transmural variation in the cardiac fiber helix angle. Among ultrasound modes are shear wave imaging (SWI) [92], elastic tensor imaging [105], and backscatter tensor imaging [49].

Histology

Histological studies of the mammalian, LV fiber orientation were first studied by fiber dissections and histologic measurements in transmural plugs of LV tissue [40, 106–109]. Principle conclusions of this work were that mid-wall fibers are circumferential, while base-apex fibers were arranged in the direction on the epicardial and endocardial [50]. Histological measurements, although 2D, have provided much information about the existence of two populations of sheets differing in orientation based on the distribution of angles in LVs [110].

Table 2 Other specialized imaging methods for studying fiber orientation

Reference	Specialized imaging method	Application	Study size	Study summary
Reese et al. [101]	NMR	Cardiac necropsy specimens	—	Described an imaging technique for determining the fiber orientation.
Helm et al. [50]	DWI	Canine hearts	7	Developed a novel hypothesis-testing method to show that distinct populations of secondary and tertiary eigenvalues may be distinguished at reasonable confidence levels within the canine LV.
Sun et al. [11]	PSOCT	Rat hearts	—	Demonstrated that destruction of the birefringence nature of the fiber muscle in the infarcted heart can be observed using PSOCT.
Fleming et al. [17]	OCT	Rabbit right ventricular free-wall images	—	Proposed a method to understand the conduction system of a sample study by imaging cardiac fibers.
Lee et al. [92]	SWI	Porcine (5) and open-chest ovine (3) hearts	8	Demonstrated that SWI is capable of mapping cardiac fiber orientation in vitro and in vivo.
Wang et al. [99]	OPT	Mouse hearts	7	Demonstrated that OPT can accurately image depth-resolved fiber orientation in fresh tissue and reveal microstructural details at the histological level.
Sommer et al. [91]	SHG	Human LV myocardium	28	Identified structural parameters for a material model of the biomechanical response.

Note: NMR indicates nuclear magnetic resonance; DWI indicates diffusion-weighted imaging; PSOCT indicates polarized-sensitive optical coherence tomography; MI indicates myocardial infarction; LV indicates left ventricle or left ventricular; OCT indicates optical coherence tomography; SWI indicates shear wave imaging; OPT indicates optical polarization tomography; SHG indicates second-harmonic generation

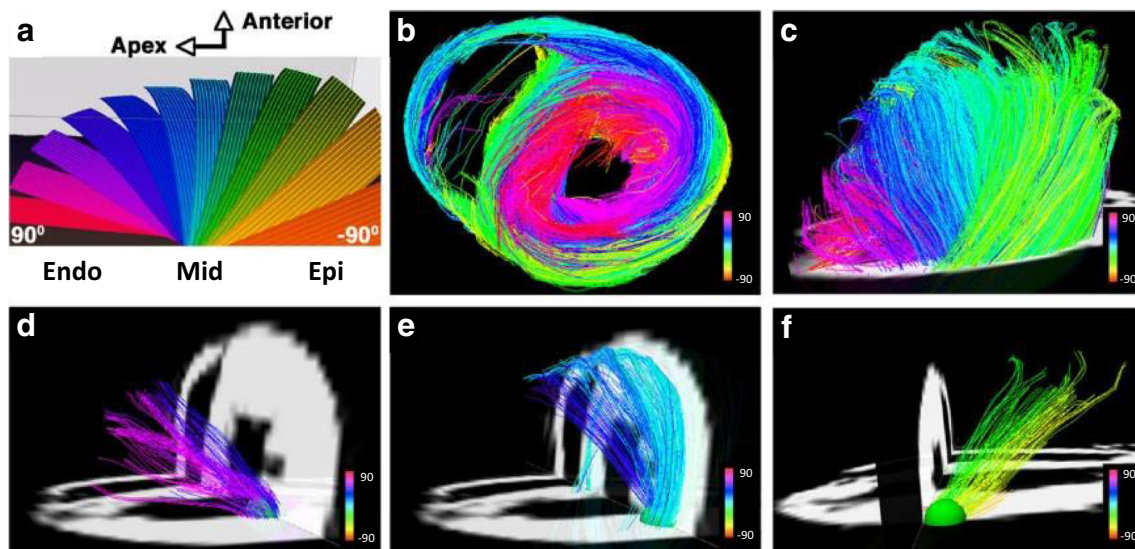


Fig. 8 DSI tractography of an *ex-vivo* normal rat heart showing the transmural variation in cardiac fiber helix angle: The LV is being viewed (a and c-f) from its lateral wall while (b) provides a short axis view. Reproduced with permission from Sosnovik et al [64].

Many theoretical analyses have been paired with histological reconstructions and share similar results. This standard technique remains as a useful way to qualitatively and directly compare results acquired from MRI and other high-resolution imaging methods [50, 78]. Histology results highlight the utility and validity of measuring cardiac fiber architecture changes linked to electrical or mechanical dysfunction. Figure 9 shows a histological section of a healthy pig heart.

Applications

Over the past 40 years, there has been remarkable progress in understanding HF [111]. More specifically, being able to “photograph” the heart has been groundbreaking for visualizing the structure of the heart and arousing the interest for more information regarding its functionality.

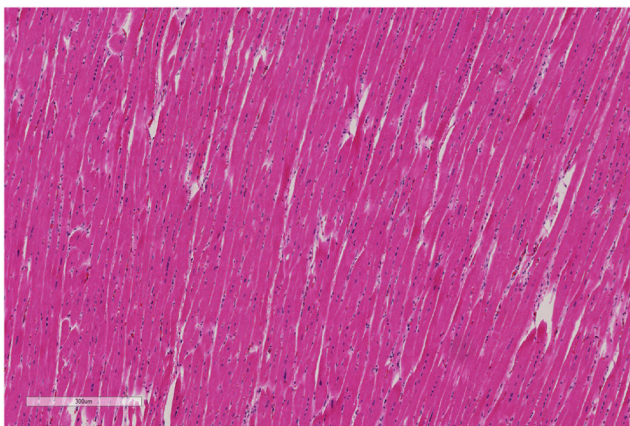


Fig. 9 Representative histological section of a healthy pig heart showing the nuclei (blue) and cardiac fibers (pink)

New methodologies which can be used to acquire myocardial orientations for patient-specific simulations of cardiac function are highly desirable. In order to address this need, Vadakkumpadan et al. hypothesized that LV fiber orientations of a normal or failing heart can be estimated from an atlas in which the geometry of the heart and fiber orientations are readily available [79]. A major limitation of their study was that human heart images were not available. Their methodology estimated fiber orientation using canine images and, admittedly, the method was not sufficiently advanced to be able to determine the accuracy of the fiber orientation estimation.

Histology and imaging modalities such as OCT and SHG have procedures, such as dehydration and fixation, and cannot directly translate to *in vivo* imaging. However, cellular and subcellular structure morphologies can be determined using SHG imaging of the muscle samples without fluorescent labeling and sectioning techniques. SHG has optical sectioning capabilities that make it very useful for determining rotations or changes in orientation and organization. It may also yield functional information regarding the physiological state of a specimen [112] due to its strong recognition of non-centrosymmetric structures. This technique can be used for studying anomalous structures [112], although it has not been frequently used in HF.

Discerning the link between structure and function of the heart can lead to the development of computational models which can assimilate all imaging information for planning of proper therapeutic strategies for a specific patient [113]. One of the ultimate goals of HF treatment is intended to be cardiac repair through regeneration of the myocardium after injury. The heart is one of the least regenerative organs in the human body, although postnatal hearts undergo some degree of cardiomyocyte renewal during normal aging and disease [1].

Although medical imaging has been proven to be powerful, using it to determine heart functionality and the severity of disease can be challenging. For example, histological studies cannot assess tissue microstructure in intact organs or in vivo. Histology can easily damage the tissue and only provides 2D stacks. Using this method to evaluate LV cardiac fiber geometry and orientation was pioneered by Nielsen et al. [114] and with a maximum attained resolution of 500 μm . MR-DTI emerged and surpassed Nielsen's early approach with its improved resolution.

MR-DTI definitely provides a better tool for characterizing cardiac fiber architecture, although it also has limitations. Some limitations of DTI-tractography include its spatial resolution (0.1–1 mm) and inability to resolve molecular signatures in the tissue imaged [115]. Continued improvements in the technology of MR-DTI will overcome the shortcomings of the diffusion tensor for representing complex white matter architecture such as crossing fibers [116].

It is also important to note that combined imaging approaches can be very beneficial. OCT/TPM introduces properties such as absorption, birefringence, scattering, and fluorescence to characterize the cellular and molecular composition of the tissue, and thus making it possible to visualize myocytes and collagen fibers [115]. MR-DTI is unable to characterize tissues at the molecular level because it lacks microscopic resolution [115].

Despite therapeutic advances, the prognosis for HF is still poor [117, 118]. Ultrasound has done an exceptional job of portraying the anisotropic characteristics of muscle [103] and enabling a better understanding of the mechanisms leading to HF as well as a greater understanding of the efficient therapeutic approach [119]. Estimating cardiac fiber orientations from 3D ultrasound images can be extended to the clinical application of examining a patient's heart [16]. Clinical implications for the measurement of ultrasonic anisotropy leads to defining the normal and pathologic cardiac structure and function and can be done in real time at a patient's bedside [49].

Overall, imaging methods have been useful for studying particular molecular and physiological changes. Improvement of imaging techniques and innovation of specific disease-mimicking conditions constitute the empirical approach to observing and understanding human disease [1].

Discussion and future directions

In recent years, cardiac fibers were shown to describe empirical observations that were linked to a particular pathological condition, although there are only a few studies that quantitate cardiac fibers in healthy human hearts versus those in early HF. To date, quantitative cardiac fiber angles have largely relied on histological imaging, modeling, and multimodality imaging. Researchers have used images from MR-DTI and

ultrasound to determine angular distribution. It can be quite interesting to determine fiber length and the number of fibers per sectioned slice of epicardium, septum, and endocardium. Most cardiac fiber studies have used multimodal imaging modalities and among those that have been used, we believe that future studies should incorporate the use of SHG to document the arrangement of cardiac fibers during HF from early to advanced states. A quantitative study that provides data regarding changes in layer-specific regions due to aging/disease is needed to better understand the pathology as well as the timeline of HF.

Conclusion

This paper provides a systematic review on various technologies for imaging cardiac fibers and HF. MR-DTI and ultrasound have been most useful and significant in the current research and clinical applications. While an increase in the interest of cardiac fiber studies exists, some of the multimodality imaging approaches used to study cardiac fibers can be complex for applications aside from research. However, this should be the direction for the research community. It would be beneficial to advance this technology in order to improve healthcare provided as current studies suggest that changes in cardiac fiber orientation may provide valuable information regarding the damage caused by the disease. Multimodal, non-linear, optical imaging of fibers also allows identification of myocardial remodeling and pathophysiological changes. New imaging technologies that have the ability to measure cardiac fiber orientations and identify structural and functional information of the heart will advance basic research and clinical diagnoses of HF.

Acknowledgements This research was supported in part by the U.S. National Institutes of Health (NIH) grants (CA176684, CA156775, and CA204254). The work was also supported in part by the Georgia Research Alliance (GRA) Distinguished Cancer Scientist Award to BF.

References

1. Santos A, Fernandez-Friera L, Villalba M, Lopez-Melgar B, Espana S, Mateo J, Mota RA, Jimenez-Borreguero J, Ruiz-Cabello J (2015) Cardiovascular imaging: what have we learned from animal models? *Front Pharmacol* 6:227. <https://doi.org/10.3389/fphar.2015.00227>
2. Helm PA, Younes L, Beg MF, Ennis DB, Leclercq C, Faris OP, McVeigh E, Kass D, Miller MI, Winslow RL (2006) Evidence of structural remodeling in the dyssynchronous failing heart. *Circ Res* 98(1):125–132. <https://doi.org/10.1161/01.RES.0000199396.30688.eb>
3. Helm P, Beg MF, Miller MI, Winslow RL (2005) Measuring and mapping cardiac fiber and laminar architecture using diffusion tensor MR imaging. *Ann N Y Acad Sci* 1047:296–307. <https://doi.org/10.1196/annals.1341.026>

4. Tseng WY, Dou J, Reese TG, Wedeen VJ (2006) Imaging myocardial fiber disarray and intramural strain hypokinesis in hypertrophic cardiomyopathy with MRI. *J Magn Reson Imaging* 23(1): 1–8. <https://doi.org/10.1002/jmri.20473>
5. Tseng WY, Wedeen VJ, Reese TG, Smith RN, Halpern EF (2003) Diffusion tensor MRI of myocardial fibers and sheets: correspondence with visible cut-face texture. *J Magn Reson Imaging* 17(1): 31–42. <https://doi.org/10.1002/jmri.10223>
6. Carreras F, Ballester M, Pujadas S, Leta R, Pons-Llado G (2006) Morphological and functional evidences of the helical heart from non-invasive cardiac imaging. *Eur J Cardiothorac Surg* 29(Suppl 1):S50–S55. <https://doi.org/10.1016/j.ejcts.2006.02.061>
7. Yeh FC, Wedeen VJ, Tseng WY (2011) Estimation of fiber orientation and spin density distribution by diffusion deconvolution. *Neuroimage* 55(3):1054–1062. <https://doi.org/10.1016/j.neuroimage.2010.11.087>
8. McLean M, Prothero J (1991) Myofiber orientation in the weanling mouse heart. *Am J Anat* 192(4):425–441. <https://doi.org/10.1002/aja.1001920410>
9. Brown NH, Dobrovolsky HM, Gauthier DJ, Wolf PD (2007) A fiber-based ratiometric optical cardiac mapping channel using a diffraction grating and split detector. *Biophys J* 93(1):254–263. <https://doi.org/10.1529/biophysj.106.101154>
10. Chen SY, Hsu CY, Sun CK (2008) Epi-third and second harmonic generation microscopic imaging of abnormal enamel. *Opt Express* 16(15):11670–11679
11. Sun CW, Wang YM, Lu LS, Lu CW, Hsu IJ, Tsai MT, Yang CC, Kiang YW, Wu CC (2006) Myocardial tissue characterization based on a polarization-sensitive optical coherence tomography system with an ultrashort pulsed laser. *J Biomed Opt* 11(5): 054016. <https://doi.org/10.1117/1.2363358>
12. Scollan DF, Holmes A, Winslow R, Forder J (1998) Histological validation of myocardial microstructure obtained from diffusion tensor magnetic resonance imaging. *Am J Phys* 275(6 Pt 2): H2308–H2318
13. Hoffman MP, Taylor EN, Aninwene GE II, Sadayappan S, Gilbert RJ (2016) Assessing the multiscale architecture of muscular tissue with Q-space magnetic resonance imaging: review. *Microsc Res Tech*. <https://doi.org/10.1002/jemt.22777>
14. Angeli S, Befera N, Peyrat JM, Calabrese E, Johnson GA, Constantinides C (2014) A high-resolution cardiovascular magnetic resonance diffusion tensor map from ex-vivo C57BL/6 murine hearts. *J Cardiovasc Magn Reson* 16:77. <https://doi.org/10.1186/s12968-014-0077-x>
15. Zhang X, Haynes P, Campbell KS, Wenk JF (2015) Numerical evaluation of myofiber orientation and transmural contractile strength on left ventricular function. *J Biomech Eng* 137(4): 044502. <https://doi.org/10.1115/1.4028990>
16. Qin X, Fei B (2015) DTI template-based estimation of cardiac fiber orientations from 3D ultrasound. *Med Phys* 42(6):2915–2924. <https://doi.org/10.1118/1.4921121>
17. Fleming CP, Ripplinger CM, Webb B, Efimov IR, Rollins AM (2008) Quantification of cardiac fiber orientation using optical coherence tomography. *J Biomed Opt* 13(3):030505. <https://doi.org/10.1117/1.2937470>
18. Lekadir K, Pashaei A, Hoogendoorn C, Pereanez M, Alba X, Frangi AF (2014) Effect of statistically derived fiber models on the estimation of cardiac electrical activation. *IEEE Trans Biomed Eng* 61(11):2740–2748. <https://doi.org/10.1109/TBME.2014.2327025>
19. Palit A, Bhudia SK, Arvanitis TN, Sherwood V, Wayte S, Turley GA, Williams MA (2015) Effect of fibre orientation on diastolic mechanics of human ventricle. *Conf Proc IEEE Eng Med Biol Soc* 2015:6523–6526. <https://doi.org/10.1109/EMBC.2015.7319887>
20. Hongo M, Ryoike T, Ross J (1997) Animal models of heart failure: recent developments and perspectives. *Trends Cardiovasc Med* 7(5):161–167
21. Kemp CD, Conte JV (2012) The pathophysiology of heart failure. *Cardiovasc Pathol* 21(5):365–371
22. Lip GYH, Gibbs CR, Beevers DG (2000) ABC of heart failure: aetiology. *BMJ* 320(7227):104–107
23. Vasan RS, Larson MG, Benjamin EJ, Evans JC, Levy D (1997) Left ventricular dilatation and the risk of congestive heart failure in people without myocardial infarction. *N Engl J Med* 336(19): 1350–1355
24. Heinzel FR, Hohendanner F, Jin G, Sedej S, Edelmann F (2015) Myocardial hypertrophy and its role in heart failure with preserved ejection fraction. *J Appl Physiol* (1985) 119(10):1233–1242. <https://doi.org/10.1152/japplphysiol.00374.2015>
25. Dai DF, Chen T, Johnson SC, Szeto H, Rabinovitch PS (2012) Cardiac aging: from molecular mechanisms to significance in human health and disease. *Antioxid Redox Signal* 16(12):1492–1526. <https://doi.org/10.1089/ars.2011.4179>
26. Kwak HB (2013) Aging, exercise, and extracellular matrix in the heart. *J Exerc Rehabil* 9(3):338–347. <https://doi.org/10.12965/jer.130049>
27. Yarbrough WM, Mukherjee R, Stroud RE, Rivers WT, Oelsen JM, Dixon JA, Eckhouse SR, Ikonomidis JS, Zile MR, Spinale FG (2012) Progressive induction of left ventricular pressure overload in a large animal model elicits myocardial remodeling and a unique matrix signature. *J Thorac Cardiovasc Surg* 143(1):215–223. <https://doi.org/10.1016/j.jtcvs.2011.09.032>
28. Eckhouse SR, Spinale FG (2012) Changes in the myocardial interstitium and contribution to the progression of heart failure. *Heart Fail Clin* 8(1):7–20. <https://doi.org/10.1016/j.hfc.2011.08.012>
29. Rodrigues PG, Leite-Moreira AF, Falcao-Pires I (2016) Myocardial reverse remodeling: how far can we rewind? *Am J Physiol Heart Circ Physiol* 310(11):H1402–H1422. <https://doi.org/10.1152/ajpheart.00696.2015>
30. Mann DL, Zipes DP, Libby P, Bonow RO (2014) Braunwald's heart disease: a textbook of cardiovascular medicine. Elsevier Health Sciences, Amsterdam
31. Vescovo G, Zennaro R, Sandri M, Carraro U, Leprotti C, Ceconi C, Ambrosio GB, Dalla Libera L (1998) Apoptosis of skeletal muscle myofibers and interstitial cells in experimental heart failure. *J Mol Cell Cardiol* 30(11):2449–2459
32. Berry C, Greenwald S (1976) Effects of hypertension on the static mechanical properties and chemical composition of the rat aorta. *Cardiovasc Res* 10(4):437–451
33. Bertoni AG, Tsai A, Kasper EK, Brancati FL (2003) Diabetes and idiopathic cardiomyopathy: a nationwide case-control study. *Diabetes Care* 26(10):2791–2795
34. Boudina S, Abel ED (2007) Diabetic cardiomyopathy revisited. *Circulation* 115(25):3213–3223
35. Chae CU, Pfeffer MA, Glynn RJ, Mitchell GF, Taylor JO, Hennekens CH (1999) Increased pulse pressure and risk of heart failure in the elderly. *JAMA* 281(7):634–643
36. Cohn JN (1999) Arterial stiffness. *J Hypertens* 17(8):1227
37. Cohn J (1999) Vascular wall function as a risk marker for cardiovascular disease. *J Hypertens Suppl* 17(5):S41–S44
38. Zile MR, Baicu CF, Gaasch WH (2004) Diastolic heart failure—abnormalities in active relaxation and passive stiffness of the left ventricle. *N Engl J Med* 350(19):1953–1959. <https://doi.org/10.1056/NEJMoa032566>
39. Mandinov L, Eberli FR, Seiler C, Hess OM (2000) Diastolic heart failure. *Cardiovasc Res* 45(4):813–825
40. Streeter DD Jr, Spotnitz HM, Patel DP, Ross J Jr, Sonnenblick EH (1969) Fiber orientation in the canine left ventricle during diastole and systole. *Circ Res* 24(3):339–347

41. Mall FP (1911) On the muscular architecture of the ventricles of the human heart. *Am J Anat* 11(3):211–266
42. Grant RP (1965) Notes on the muscular architecture of the left ventricle. *Circulation* 32(2):301–308
43. Fox JJ, Gilmour RF Jr, Bodenschatz E (2002) Conduction block in one-dimensional heart fibers. *Phys Rev Lett* 89(19):198101. <https://doi.org/10.1103/PhysRevLett.89.198101>
44. Rohmer D, Sitek A, Gullberg GT (2007) Reconstruction and visualization of fiber and laminar structure in the normal human heart from ex vivo diffusion tensor magnetic resonance imaging (DTMRI) data. *Invest Radiol* 42(11):777–789. <https://doi.org/10.1097/RLI.0b013e3181238330>
45. Savadjiev P, Strijkers GJ, Bakermans AJ, Piuze E, Zucker SW, Siddiqi K (2012) Heart wall myofibers are arranged in minimal surfaces to optimize organ function. *Proc Natl Acad Sci U S A* 109(24):9248–9253. <https://doi.org/10.1073/pnas.1120785109>
46. Qin X, Wang S, Shen M, Zhang X, Wagner MB, Fei B (2014) Mapping cardiac fiber orientations from high-resolution DTI to high-frequency 3D ultrasound. *Proc SPIE Int Soc Opt Eng* 9036: 90361O. <https://doi.org/10.1117/12.2043821>
47. Qin X, Wang S, Shen M, Zhang X, Lerakis S, Wagner MB, Fei B (2015) 3D in vivo imaging of rat hearts by high frequency ultrasound and its application in myofiber orientation wrapping. *Proc SPIE Int Soc Opt Eng* 9419. <https://doi.org/10.1117/12.2082326>
48. Sengupta PP, Korinek J, Belohlavek M, Narula J, Vannan MA, Jahangir A, Khandheria BK (2006) Left ventricular structure and function: basic science for cardiac imaging. *J Am Coll Cardiol* 48(10):1988–2001. <https://doi.org/10.1016/j.jacc.2006.08.030>
49. Wickline SA, Verdonk ED, Miller JG (1991) Three-dimensional characterization of human ventricular myofiber architecture by ultrasonic backscatter. *J Clin Invest* 88(2):438–446. <https://doi.org/10.1172/JCI115323>
50. Helm PA, Tseng HJ, Younes L, McVeigh ER, Winslow RL (2005) Ex vivo 3D diffusion tensor imaging and quantification of cardiac laminar structure. *Magn Reson Med* 54(4):850–859. <https://doi.org/10.1002/mrm.20622>
51. Fuster V, Danielson MA, Robb RA, Broadbent JC, Brown AL Jr, Elveback LR (1977) Quantitation of left ventricular myocardial fiber hypertrophy and interstitial tissue in human hearts with chronically increased volume and pressure overload. *Circulation* 55(3):504–508
52. Geerts-Ossevoort L, Bovendeerd P, Prinzen F, Arts T, Nicolay K (2001) Myofiber orientation in the normal and infarcted heart, assessed with MR-diffusion tensor imaging. In: *Computers in cardiology 2001*. IEEE, pp 621–624
53. Wu MT, Tseng WY, Su MY, Liu CP, Chiou KR, Wedeen VJ, Reese TG, Yang CF (2006) Diffusion tensor magnetic resonance imaging mapping the fiber architecture remodeling in human myocardium after infarction: correlation with viability and wall motion. *Circulation* 114(10):1036–1045. <https://doi.org/10.1161/CIRCULATIONAHA.105.545863>
54. Streeter DD Jr, Vaishnav RN, Patel DJ, Spotnitz HM, Ross J Jr, Sonnenblick EH (1970) Stress distribution in the canine left ventricle during diastole and systole. *Biophys J* 10(4):345–363. [https://doi.org/10.1016/S0006-3495\(70\)86306-8](https://doi.org/10.1016/S0006-3495(70)86306-8)
55. Lewis BS, Gotsman MS (1975) Cardiac hypertrophy and left ventricular end-diastolic stress. *Isr J Med Sci* 11(4):299–303
56. Milne ML, Singh GK, Miller JG, Holland MR (2012) Echocardiographic-based assessment of myocardial fiber structure in individual, excised hearts. *Ultrason Imaging* 34(3):129–141. <https://doi.org/10.1177/0161734612455580>
57. Zhou Y, Zheng YP (2008) Estimation of muscle fiber orientation in ultrasound images using rotating hough transform (RVHT). *Ultrasound Med Biol* 34(9):1474–1481. <https://doi.org/10.1016/j.ultrasmedbio.2008.02.009>
58. Zhou Y, Zheng Y-P (2009) Enhancement of muscle fibers in ultrasound images using Gabor filters. In: 2009 I.E. International Ultrasonics Symposium. IEEE, pp 2296–2299
59. Quandt D, Knirsch W, Niesse O, Schraner T, Dave H, Kretschmar O (2013) Impact of chest X-ray before discharge in asymptomatic children after cardiac surgery—prospective evaluation. *Pediatr Cardiol* 34(1):155–158. <https://doi.org/10.1007/s00246-012-0405-6>
60. Gadsbøll N, Høilund-Carlsen P, Nielsen G, Berning J, Brunn N, Stage P, Hein E, Marving J, Løngborg-Jensen H, Jensen B (1989) Symptoms and signs of heart failure in patients with myocardial infarction: reproducibility and relationship to chest X-ray, radionuclide ventriculography and right heart catheterization. *Eur Heart J* 10(11):1017–1028
61. Grossman W (1986) Profiles in valvular heart disease. Lea and Febiger, United States
62. Tei C, Nishimura RA, Seward JB, Tajik AJ (1997) Noninvasive Doppler-derived myocardial performance index: correlation with simultaneous measurements of cardiac catheterization measurements. *J Am Soc Echocardiogr* 10(2):169–178
63. O'Dell WG, McCulloch AD (2000) Imaging three-dimensional cardiac function. *Annu Rev Biomed Eng* 2:431–456. <https://doi.org/10.1146/annurev.bioeng.2.1.431>
64. Sosnovik DE, Wang R, Dai G, Reese TG, Wedeen VJ (2009) Diffusion MR tractography of the heart. *J Cardiovasc Magn Reson* 11:47. <https://doi.org/10.1186/1532-429X-11-47>
65. Han BK, Lesser JR (2013) CT imaging in congenital heart disease: an approach to imaging and interpreting complex lesions after surgical intervention for tetralogy of Fallot, transposition of the great arteries, and single ventricle heart disease. *J Cardiovasc Comput Tomogr* 7(6):338–353. <https://doi.org/10.1016/j.jcct.2013.10.003>
66. Ropers D, Baum U, Pohle K, Anders K, Ulzheimer S, Ohnesorge B, Schlundt C, Bautz W, Daniel WG, Achenbach S (2003) Detection of coronary artery stenoses with thin-slice multi-detector row spiral computed tomography and multiplanar reconstruction. *Circulation* 107(5):664–666
67. Bengel FM, Higuchi T, Javadi MS, Lautamäki R (2009) Cardiac positron emission tomography. *J Am Coll Cardiol* 54(1):1–15
68. Eitzman D, Al-Aouar Z, Kanter HL, vom Dahl J, Kirsh M, Deeb GM, Schwaiger M (1992) Clinical outcome of patients with advanced coronary artery disease after viability studies with positron emission tomography. *J Am Coll Cardiol* 20(3):559–565
69. Kajander S, Joutsiniemi E, Saraste M, Pietilä M, Ukkonen H, Saraste A, Sipilä H, Teräs M, Mäki M, Airaksinen J (2010) Cardiac positron emission tomography/computed tomography imaging accurately detects anatomically and functionally significant coronary artery. *DiseaseCLINICAL PERSPECTIVE. Circulation* 122(6):603–613
70. Keyes JW, Leonard PF, Brody SL, Svetkoff DJ, Rogers WL, Lucchesi BR (1978) Myocardial infarct quantification in the dog by single photon emission computed tomography. *Circulation* 58(2):227–232
71. Gussenhoven EJ, Essed CE, Lancée CT, Mastik F, Frietman P, van Egmond FC, Reiber J, Bosch H, van Urk H, Roelandt J (1989) Arterial wall characteristics determined by intravascular ultrasound imaging: an in vitro study. *J Am Coll Cardiol* 14(4):947–952
72. Nissen SE, Gurley JC, Grines CL, Booth DC, McClure R, Berk M, Fischer C, DeMaria AN (1991) Intravascular ultrasound assessment of lumen size and wall morphology in normal subjects and patients with coronary artery disease. *Circulation* 84(3):1087–1099
73. Izumi S, Miyatake K, Beppu S, Park YD, Nagata S, Kinoshita N, Sakakibara H, Nimura Y (1987) Mechanism of mitral regurgitation in patients with myocardial infarction: a study using real-time

- two-dimensional Doppler flow imaging and echocardiography. *Circulation* 76(4):777–785
74. Khalil MM, Tremoleda JL, Bayomy TB, Gsell W (2011) Molecular SPECT imaging: an overview. *Int J Mol Imaging* 2011:796025. <https://doi.org/10.1155/2011/796025>
 75. Seidell JC, Bakker CJ, van der Kooy K (1990) Imaging techniques for measuring adipose-tissue distribution—a comparison between computed tomography and 1.5-T magnetic resonance. *Am J Clin Nutr* 51(6):953–957
 76. Chen J, Liu W, Zhang H, Lacy L, Yang X, Song SK, Wickline SA, Yu X (2005) Regional ventricular wall thickening reflects changes in cardiac fiber and sheet structure during contraction: quantification with diffusion tensor MRI. *Am J Physiol Heart Circ Physiol* 289(5):H1898–H1907. <https://doi.org/10.1152/ajpheart.00041.2005>
 77. Qin X, Wang S, Shen M, Zhang X, Lerakis S, Wagner MB, Fei B (2015) Register cardiac fiber orientations from 3D DTI volume to 2D ultrasound image of rat hearts. *Proc SPIE Int Soc Opt Eng* 9415. <https://doi.org/10.1117/12.2082317>
 78. Hsu EW, Muzikant AL, Matulevicius SA, Penland RC, Henriquez CS (1998) Magnetic resonance myocardial fiber-orientation mapping with direct histological correlation. *Am J Phys* 274(5 Pt 2):H1627–H1634
 79. Vadakkumpadan F, Arevalo H, Ceritoglu C, Miller M, Trayanova N (2012) Image-based estimation of ventricular fiber orientations for personalized modeling of cardiac electrophysiology. *IEEE Trans Med Imaging* 31(5):1051–1060. <https://doi.org/10.1109/TMI.2012.2184799>
 80. Healy LJ, Jiang Y, Hsu EW (2011) Quantitative comparison of myocardial fiber structure between mice, rabbit, and sheep using diffusion tensor cardiovascular magnetic resonance. *J Cardiovasc Magn Reson* 13:74. <https://doi.org/10.1186/1532-429X-13-74>
 81. Crosby J, Hergum T, Remme EW, Torp H (2009) The effect of including myocardial anisotropy in simulated ultrasound images of the heart. *IEEE Trans Ultrason Ferroelectr Freq Control* 56(2):326–333. <https://doi.org/10.1109/TUFC.2009.1041>
 82. Kung GL, Nguyen TC, Itoh A, Skare S, Ingels NB Jr, Miller DC, Ennis DB (2011) The presence of two local myocardial sheet populations confirmed by diffusion tensor MRI and histological validation. *J Magn Reson Imaging* 34(5):1080–1091. <https://doi.org/10.1002/jmri.22725>
 83. Merchant SS, Gomez AD, Morgan JL, Hsu EW (2016) Parametric modeling of the mouse left ventricular myocardial fiber structure. *Ann Biomed Eng* 44(9):2661–2673. <https://doi.org/10.1007/s10439-016-1574-x>
 84. Stankovic Z, Blanke P, Markl M (2012) Usefulness of 4D MRI flow imaging to control TIPS function. *Am J Gastroenterol* 107(2):327–328. <https://doi.org/10.1038/ajg.2011.380>
 85. Stankovic Z, Allen BD, Garcia J, Jarvis KB, Markl M (2014) 4D flow imaging with MRI. *Cardiovasc Diagn Ther* 4(2):173–192. <https://doi.org/10.3978/j.issn.2223-3652.2014.01.02>
 86. Karlou WJ, Covell JW, McCulloch AD, Hunter JJ, Omens JH (1998) Automated measurement of myofiber disarray in transgenic mice with ventricular expression of ras. *Anat Rec* 252(4):612–625. [https://doi.org/10.1002/\(SICI\)1097-0185\(199812\)252:4<612::AID-AR12>3.0.CO;2-1](https://doi.org/10.1002/(SICI)1097-0185(199812)252:4<612::AID-AR12>3.0.CO;2-1)
 87. Ashikaga H, Coppola BA, Hopfenfeld B, Leifer ES, McVeigh ER, Omens JH (2007) Transmural dispersion of myofiber mechanics: implications for electrical heterogeneity in vivo. *J Am Coll Cardiol* 49(8):909–916
 88. Gan Y, Tsay D, Amir SB, Marboe CC, Hendon CP (2016) Automated classification of optical coherence tomography images of human atrial tissue. *J Biomed Opt* 21(10):101407. <https://doi.org/10.1117/1.JBO.21.10.101407>
 89. Dormer J, Qin X, Shen M, Wang S, Zhang X, Jiang R, Wagner MB, Fei B (2016) Determining cardiac fiber orientation using FSL and registered ultrasound/DTI volumes. *Proc SPIE Int Soc Opt Eng* 9790. <https://doi.org/10.1117/12.2217296>
 90. Qin X, Cong Z, Jiang R, Shen M, Wagner MB, Kishbom P, Fei B (2013) Extracting cardiac Myofiber orientations from high frequency ultrasound images. *Proc SPIE Int Soc Opt Eng* 8675. <https://doi.org/10.1117/12.2006494>
 91. Sommer G, Schriefl AJ, Andra M, Sacherer M, Viertler C, Wolinski H, Holzapfel GA (2015) Biomechanical properties and microstructure of human ventricular myocardium. *Acta Biomater* 24:172–192. <https://doi.org/10.1016/j.actbio.2015.06.031>
 92. Lee WN, Pernot M, Couade M, Messas E, Bruneval P, Bel A, Hagege AA, Fink M, Tanter M (2012) Mapping myocardial fiber orientation using echocardiography-based shear wave imaging. *IEEE Trans Med Imaging* 31(3):554–562. <https://doi.org/10.1109/TMI.2011.2172690>
 93. Beg MF, Helm PA, McVeigh E, Miller MI, Winslow RL (2004) Computational cardiac anatomy using MRI. *Magn Reson Med* 52(5):1167–1174. <https://doi.org/10.1002/mrm.20255>
 94. Lekadir K, Ghafaryasl B, Munoz-Moreno E, Butakoff C, Hoogendoorn C, Frangi AF (2011) Predictive modeling of cardiac fiber orientation using the Knutsson mapping. *Med Image Comput Assist Interv* 14(Pt 2):50–57
 95. Genet M, Lee LC, Nguyen R, Haraldsson H, Acevedo-Bolton G, Zhang Z, Ge L, Ordovas K, Kozerke S, Guccione JM (2014) Distribution of normal human left ventricular myofiber stress at end diastole and end systole: a target for in silico design of heart failure treatments. *J Appl Physiol* (1985) 117(2):142–152. <https://doi.org/10.1152/jappphysiol.00255.2014>
 96. Qin X, Fei B (2014) Measuring myofiber orientations from high-frequency ultrasound images using multiscale decompositions. *Phys Med Biol* 59(14):3907–3924. <https://doi.org/10.1088/0031-9155/59/14/3907>
 97. Qin X, Wang S, Shen M, Lu G, Zhang X, Wagner MB, Fei B (2015) Simulating cardiac ultrasound image based on MR diffusion tensor imaging. *Med Phys* 42(9):5144–5156. <https://doi.org/10.1118/1.4927788>
 98. Gilbert SH, Benson AP, Li P, Holden AV (2007) Regional localisation of left ventricular sheet structure: integration with current models of cardiac fibre, sheet and band structure. *Eur J Cardiothorac Surg* 32(2):231–249. <https://doi.org/10.1016/j.ejcts.2007.03.032>
 99. Wang Y, Zhang K, Wasala N, Yao X, Duan D, Yao G (2014) Histology validation of mapping depth-resolved cardiac fiber orientation in fresh mouse heart using optical polarization tractography. *Biomedical optics express* 5(8):2843–2855
 100. Buckberg G, Mahajan A, Saleh S, Hoffman JI, Coghlan C (2008) Structure and function relationships of the helical ventricular myocardial band. *J Thorac Cardiovasc Surg* 136(3):578–589. <https://doi.org/10.1016/j.jtcvs.2007.10.088>
 101. Reese TG, Weisskoff RM, Smith RN, Rosen BR, Dinsmore RE, Wedeen VJ (1995) Imaging myocardial fiber architecture in vivo with magnetic resonance. *Magn Reson Med* 34(6):786–791
 102. Yip G, Abraham T, Belohlavek M, Khandheria BK (2003) Clinical applications of strain rate imaging. *J Am Soc Echocardiogr* 16(12):1334–1342. <https://doi.org/10.1067/j.echo.2003.09.004>
 103. Aygen M, Popp RL (1987) Influence of the orientation of myocardial fibers on echocardiographic images. *Am J Cardiol* 60(1):147–152
 104. Denslow S, Balaji S, Hewett KW (2000) A new framework for echocardiographic assessment of left ventricular mechanics: sensitivity to heart failure. *J Am Soc Echocardiogr* 13(11):969–979
 105. Lee W-N, Larrat B, Pernot M, Tanter M (2012) Ultrasound elastic tensor imaging: comparison with MR diffusion tensor imaging in the myocardium. *Phys Med Biol* 57(16):5075–5095

106. Streeter DD Jr, Hanna WT (1973) Engineering mechanics for successive states in canine left ventricular myocardium. II. Fiber angle and sarcomere length. *Circ Res* 33(6):656–664
107. Ross AA, Streeter DD Jr (1979) Myocardial fiber disarray. *Circulation* 60(6):1425–1426
108. Streeter DD (1979) Gross morphology and fiber geometry of the heart. *Handbook of Physiology*, 61–112
109. Streeter DD, Ramon C (1983) Muscle pathway geometry in the heart wall. *J Biomech Eng* 105(4):367–373
110. Arts T, Costa KD, Covell JW, McCulloch AD (2001) Relating myocardial laminar architecture to shear strain and muscle fiber orientation. *Am J Physiol Heart Circ Physiol* 280(5):H2222–H2229
111. Katz AM (2008) The “modern” view of heart failure how did we get here? *Circ Heart Fail* 1(1):63–71
112. Both M, Vogel M, Friedrich O, von Wegner F, Ku T, Fink RH, Uttenweiler D (2004) Second harmonic imaging of intrinsic signals in muscle fibers in situ. *J Biomed Opt* 9(5):882–892
113. Hunter P, Nielsen P (2005) A strategy for integrative computational physiology. *Physiology (Bethesda)* 20:316–325. <https://doi.org/10.1152/physiol.00022.2005>
114. Nielsen PM, Le Grice IJ, Smaill BH, Hunter PJ (1991) Mathematical model of geometry and fibrous structure of the heart. *Am J Phys* 260(4 Pt 2):H1365–H1378
115. Goergen CJ, Chen HH, Sakadžić S, Srinivasan VJ, Sosnovik DE (2016) Microstructural characterization of myocardial infarction with optical coherence tractography and two-photon microscopy. *Physiol Rep* 4(18):e12894
116. Mukherjee P, Chung SW, Berman JJ, Hess CP, Henry RG (2008) Diffusion tensor MR imaging and fiber tractography: technical considerations. *AJNR Am J Neuroradiol* 29(5):843–852. <https://doi.org/10.3174/ajnr.A1052>
117. Gronda E, Mangiavacchi M, Andreuzzi B, Municino A (2001) Arrhythmia risk stratification in patients with heart failure according to drug treatment and its effects. *Ital Heart J Suppl* 2(12):1278–1283
118. Farmakis D, Parissis J, Lekakis J, Filippatos G (2015) Acute heart failure: epidemiology, risk factors, and prevention. *Rev Esp Cardiol (Engl Ed)* 68(3):245–248. <https://doi.org/10.1016/j.rec.2014.11.004>
119. Dalla-Volta S, Razzolini R, Scognamiglio R, Rubino A, Chioin R (1988) Myocardial function in heart failure. *Cardiology* 75(Suppl 1):8–18